NANO LETTERS

pubs.acs.org/NanoLett

Letter

Mechanical Tester Driven by Surface Tension

Yan Wang,* Biqi Shao, Jia Song, Wei Hong,* and Chuan Fei Guo*

Cite This: *Nano Lett.* 2024, 24, 4012−4019

Read Online

ACCESS | Metrics & More | Article Recommendations | Supporting Information

ABSTRACT: The measurement of in-plane mechanical properties, such as Young's modulus and strength, of thin and stretchable materials has long been a challenge. Existing measurements, including wrinkle instability and nano indentation, are either indirect or destructive, and are inapplicable to meshes or porous materials, while the conventional tension test fails to measure the mechanical properties of nanoscale films. Here, we report a technique to test thin and stretchable films by loading a thin film afloat via differential surface tension and recording its deformation. We have demonstrated the method by measuring the Young's moduli of homogeneous films of soft materials including polydimethylsiloxane and Ecoflex and verified the results with known values. We further measured the strain distributions of meshes, both isotropic and anisotropic, which were otherwise nearly impossible to measure. The method proposed herein is expected to be generally applicable to many material systems that are thin, stretchable, and water-insoluble.

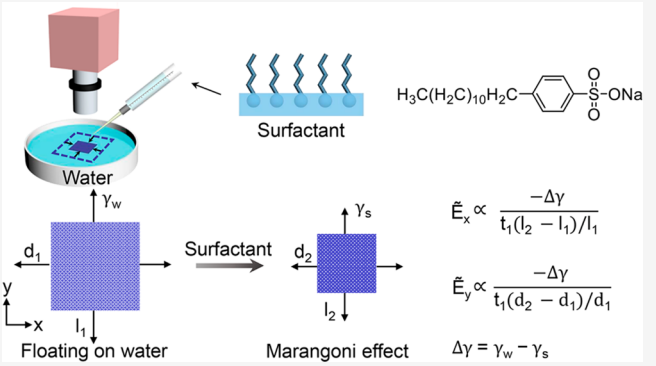

KEYWORDS: *Marangoni effect, surface tension, Young's modulus, measurement, free-standing film*

Stretchable electronics is an emerging field revolutionizing the ways that robots interact with the environment and humans monitor their health.[1−4] One of the key problems along this direction is to accurately measure the mechanical properties (such as modulus and strength) of soft and thin materials in the devices—this facilitates the design and fabrication of flexible devices, as well as their integration on biotissues[5,6] and soft robots[7,8] because a mechanical mismatch often leads to an unstable interface and thus limited lifetime.[9−11] In bioelectronics, a material laminated on the skin or implanted in the body should have a stiffness close to that of the biotissue for conformal and long-term integration.[6,12,13] Metals and semiconductors, on the other hand, are often made porous or mesh-like to achieve high stretchability.[14−17] However, determination of the mechanical properties of such materials remains challenging.

While conventional mechanical tests may not be applicable to such thin and stretchable films or membranes, there have been several methods to measure the elastic properties of continuous thin layers. An indirect method is to place a thin material on a soft substrate and buckle the bilayer by heating or releasing from a prestretched status, and its modulus can be determined from the wavelength of surface wrinkles.[18−20] However, this method is unsuitable for heterogeneous materials and the mechanical properties might be affected by the interfacial adhesion between film and substrate.[21,22] Another method is to deform a free-standing film out of plane by a nanoindentor or applying a pressure,[23−27] or applying an in-plane load through microscopic devices.[28,29] Such methods, however, need to grow or transfer the materials on a nanoscale gap or well. The manipulation is complicated and requires expensive facilities (e.g., atomic force microscope,[23,25] scanning electron microscope,[28−30] nanoindentor[26,27]) and well-trained operators. The measurements may also be affected by the adhesion between the material and the supporting substrate.[31−33] Furthermore, nanoindentation and bulge tests cannot be directly applied to a nanomesh or a nanoporous film.

The Marangoni effect is a phenomenon that a differential surface tension is imposed to a floating object, leading to the motion or deformation of the object.[34,35] In this work, we use the Marangoni effect to characterize the in-plane mechanical properties of stretchable thin layers floating on water including soft membranes, meshes, and porous films. We have established models for the measurement based on the change in surface tension of water that deforms the floating object and further verified the effectiveness of the model by comparing the measured moduli of polydimethylsiloxane (PDMS, Sylgard 184) and Ecoflex (0010, Smooth-On) to known results. We

Received: February 7, 2024
Revised: March 20, 2024
Accepted: March 20, 2024
Published: March 25, 2024

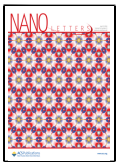

https://doi.org/10.1021/acs.nanolett.4c00702
Nano Lett. 2024, 24, 4012−4019

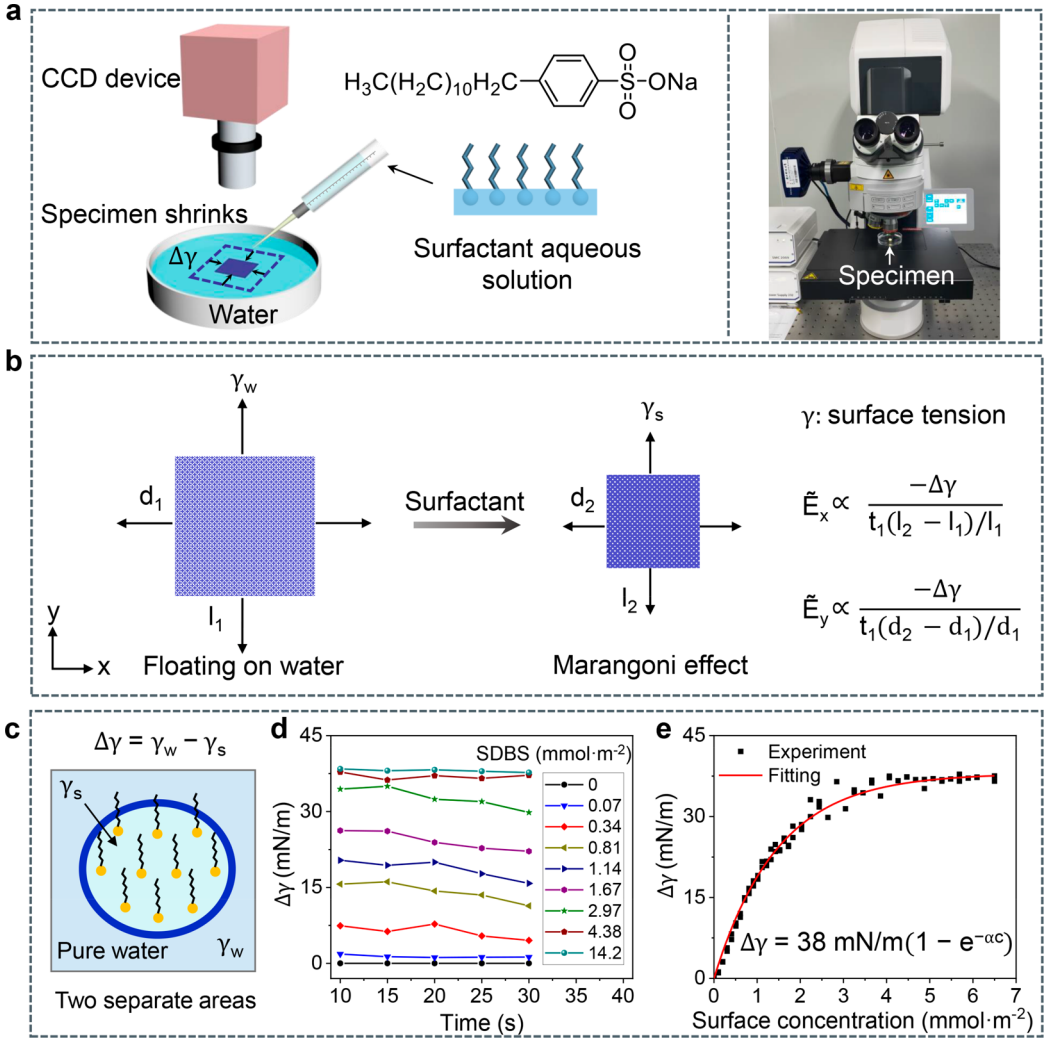

Figure 1. Principle for the Marangoni-effect-based measurement of mechanical properties. (a) Principle of the measurement. (b) The measurement of biaxial stiffness. The sample thickness t_1 is calculated from the as-prepared value by considering the areal expansion. (c) The two regions of water, with the closed region being added with SDBS molecules to reduce its surface tension. (d) Stabilized surface tension difference between the two separate regions with time. At an SDBS concentration of 14.2 mmol·m^{-2}, the surface tension difference is stable over at least 20 s. (e) Surface tension difference as a function of the surface concentration of SDBS.

also show that our method can measure the in-plane mechanical properties (e.g., elastic modulus and shear strength) of nanomeshes, both isotropic and anisotropic. The Marangoni-effect-based method can be conducted at the macroscale without the use of a high-precision microscope or a nanoindenter and is effective across scales. This method is also expected to measure the in-plane mechanical properties of many other materials, assemblies, and structures that are highly deformable and floatable on a liquid.

PRINCIPLE OF THE MARANGONI-EFFECT-BASED MEASUREMENT

Our method needs to introduce a surface-tension difference between the two sides of a thin layer afloat. Water was selected as the carrying liquid due to two factors. First, water is a stable and safe liquid that has a high surface tension of ~72 mN·m^{-1}, the largest among commonly seen nonmetallic liquids. The large surface tension provides a large space to tailor the surface tension (by simply adding a surfactant) to generate a large tension difference. Second, the viscosity of water is only 1.0 mPa·s, which causes negligible friction when a floating specimen is being deformed (Figure S1). As a result, a floating film is considered to be free-standing during the measurement.

The driving force of the method is the differential surface tension $\Delta\gamma$ between the two sides of the floating specimen, $\Delta\gamma = \gamma_w - \gamma_s$, where γ_w and γ_s are the surface tensions of pure water and water with surfactants, respectively. The testing procedure of the floating specimen is shown in Figure 1a. Before adding any surfactant, the lateral dimensions of specimen $l_1 \times d_1$ were captured using a charge-coupled device (CCD) camera, and the thickness t_1 was calculated from the as-prepared value by considering the areal expansion. After equilibrium is established, an aqueous surfactant solution, sodium dodecylbenzenesulfonate (SDBS), is dropwise added to the water surface. The Janus SDBS molecules diffuse quickly on the water surface, and the surface tension decreases substantially (Figure S2), resulting in the shrinkage of the specimen. The effective biaxial stiffnesses along the x- and y-direction can be obtained as $\tilde{E}_x = -\Delta\gamma/t_1\epsilon_x$ and $\tilde{E}_y = -\Delta\gamma/t_1\epsilon_y$. The engineering strains $\epsilon_x = \frac{l_2 - l_1}{l_1}$ and $\epsilon_y = \frac{d_2 - d_1}{d_1}$, with l_2 and

https://doi.org/10.1021/acs.nanolett.4c00702
Nano Lett. 2024, 24, 4012−4019

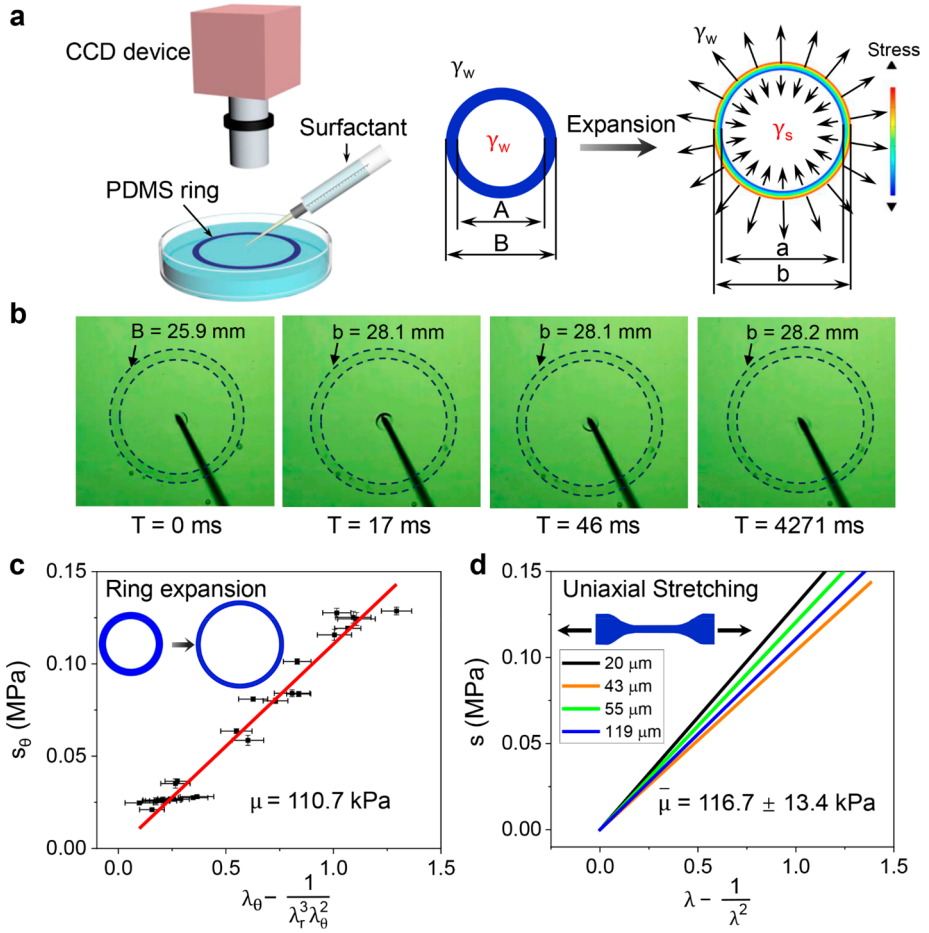

Figure 2. Verification of the effectiveness of the Marangoni-effect-based measurement. (a) A ring-expansion test. (b) Dynamic expansion of the PDMS ring after a drop of SDBS is added in the inner region of the ring. States at times (T) of 0, 17, 46, and 4271 ms are shown. (c) Relation between the nominal hoop stress s_θ and the reduced strain $\lambda_\theta - \frac{1}{\lambda_r^3\lambda_\theta^2}$. (d) Nominal axial stress s and reduced stretch $\lambda - \frac{1}{\lambda^2}$ curve of PDMS film measured using conventional uniaxial tension tests.

d_2 being the length and width at equilibrium after surfactant addition, respectively, are shown in Figure 1b.

Generating a sufficiently large surface tension difference to deform the specimen is a key step of the proposed method. The surface tension of liquids can be measured by the Du Nouy ring method[36] (Figure S3). Surfactant molecules preferentially arrange on the water surface rather than diffuse inside water. Therefore, a specimen afloat separating the surface into discontinuous regions effectively keeps the surfactant molecules only in the intended region, thus generating differential surface tension. For example, a floating annulus specimen will experience decreased surface tension from the inner region, in which a surfactant is added, while the tension over the other boundary is unchanged, as illustrated in Figure 1c. The differential surface tension is stable for ~20 s (Figure 1d), allowing deformation measurements through common imaging methods.

Unlike the dead loads in a conventional mechanical test, the loads applied through the surface tension vary with the deformed length of a boundary. For example, the difference in the nominal stress Δs induced by $\Delta\gamma$, along an edge of stretch λ in the tangential direction, can be written as $\Delta s = \Delta\gamma\lambda/t$, with t being the thickness prior to the surfactant addition. The differential surface tension $\Delta\gamma$ is tuned by controlling the SDBS concentration. Figure 1e plots $\Delta\gamma$ as a function of the surface concentration of SDBS c, which can be approximated by an empirical relation, $\Delta\gamma = 38\ \text{mN/m}(1 - e^{-\alpha c})$, with $\alpha = 0.68\ \text{m}^2\ \text{mmol}^{-1}$. The repeatability of the result ensures precise control of the load by the added volume of the SDBS solution.

VERIFICATION OF THE MEASUREMENT

We used stretchable materials (PDMS and Ecoflex) with known moduli to verify the proposed method. The elastic modulus of PDMS can vary from tens of kilopascals to a few megapascals by tuning the weight ratio of the base to the curing agent. The change in the surface tension of water may induce a large deformation in a PDMS film afloat. An annulus PDMS film (the thickness is 3.11 μm) was used in the tests. Topped by a thin layer of SDBS solution, the surface surrounded by the ring exhibits a lower tension and the PDMS ring expands uniformly within 0.1 s. Equilibrium is stablished within tens of milliseconds and remains stable for a few seconds, as shown in Figure 2a,b and Movie S1. Images before and after deformation of the ring were captured by the camera.

Each material particle in the expanded ring is stretched biaxially. Because the width of the ring is far smaller than its diameter, an approximately uniform deformation is assumed,[37] and the principal stretches along the radial (λ_r) and circumferential directions (λ_θ) are estimated as

https://doi.org/10.1021/acs.nanolett.4c00702
Nano Lett. 2024, 24, 4012−4019

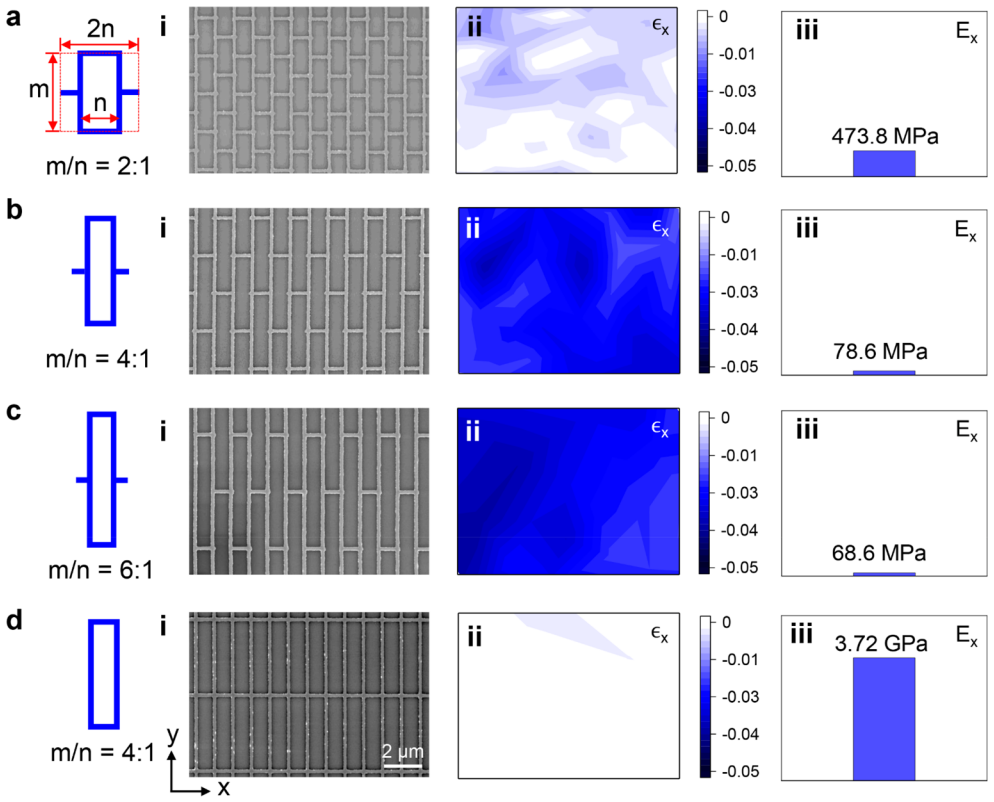

Figure 3. Measurement of Young's moduli of ordered 2D nanomeshes. (a–c) Ordered meshes with staggered unit cells (aspect ratio m/n = 2, 4, and 6 for panel a, b, and c, respectively; n = 1 μm) and measured Young's moduli. (d) Nanomesh structure with nonstaggered rectangles (m/n = 4). Column (i) shows SEM images of the Au nanomeshes. Column (ii) shows compressive strain distributions of the Au nanomeshes in the x-direction. Column (iii) shows the measured Young's moduli of the Au nanomeshes in the x-direction.

$$\lambda_r = \frac{b-a}{B-A}, \qquad \lambda_\theta = \frac{a+b}{A+B} \tag{1}$$

Here, A and B are the inner and outer radii of the ring before expansion, respectively, and a and b are the corresponding radii in the expanded state (detailed data are shown in Table S1). The through-thickness stretch $\lambda_z = 1/\lambda_r\lambda_\theta$ is calculated from the volume incompressibility.

On the other hand, the average nominal hoop stress is estimated as

$$s_\theta \approx \frac{\gamma_w b - \gamma_s a}{t(B-A)} \tag{2}$$

Generally, the constitutive relation of an isotropic rubbery material is expressed in terms of the free energy density $W = W(I_1)$, where $I_1 = \lambda_1^2 + \lambda_2^2 + \lambda_3^2$ is the first invariant of the deformation tensor. Subject to biaxial tension with in-plane principal stretches λ_r and λ_θ, the stress–stretch relation can then be written as

$$s_\theta = 2\frac{dW}{dI_1}\left(\lambda_\theta - \frac{1}{\lambda_r^3\lambda_\theta^2}\right) \tag{3}$$

The experimental data, in terms of the nominal hoop stress s_θ and the reduced strain $\lambda_\theta - 1/\lambda_r^3\lambda_\theta^2$, are plotted in Figure 2c. An approximately linear relation between the nominal stress and the reduced strain is observed for specimens at different thicknesses, indicating that the material can be well characterized by the neo-Hookean model.[38] The shear modulus μ of the PDMS is then determined from the slope of the curve

$$\mu = 2\frac{dW}{dI_1} \approx 110.7 \text{ kPa} \tag{4}$$

We further established a finite-element model for the field of deformation in the annulus ring subjected to nonequal line forces on the inner and outer perimeters. A neo-Hookean material of initial shear modulus μ = 100 kPa is used in the simulation. The averaged stress–stretch relation is evaluated from the simulation and compared with the relation directly from the material model in Figure S4. A good agreement has been reached under relatively small deformations.

The elastic modulus of PDMS is often regarded as thickness independent for films thicker than 600 nm,[39] while that of thicker samples can be determined through conventional tests. Here, for comparison, thicker PDMS specimens (of thicknesses 20, 43, 55, and 119 μm) were prepared and subjected to uniaxial tension tests over a dynamic mechanical analysis (DMA) machine, and the results are shown in Figure 2d. From the results, the average shear modulus of PDMS by a uniaxial tension test is determined to be 116.7 ± 13.4 kPa, which is in good agreement with our method (110.7 kPa). Likewise, Ecoflex 0010, a softer elastomer, is also used for the verification. The Young's modulus of Ecoflex 0010 has also been measured using our method and traditional method, and there is little difference between the results (Figure S5 and Table S2). These results all demonstrate the effectiveness and reliability of the proposed surface-tension-driven measurement. Note that the unique liquid-surface environment of the method, without expensive and high-precision equipment, is

https://doi.org/10.1021/acs.nanolett.4c00702
Nano Lett. 2024, 24, 4012–4019

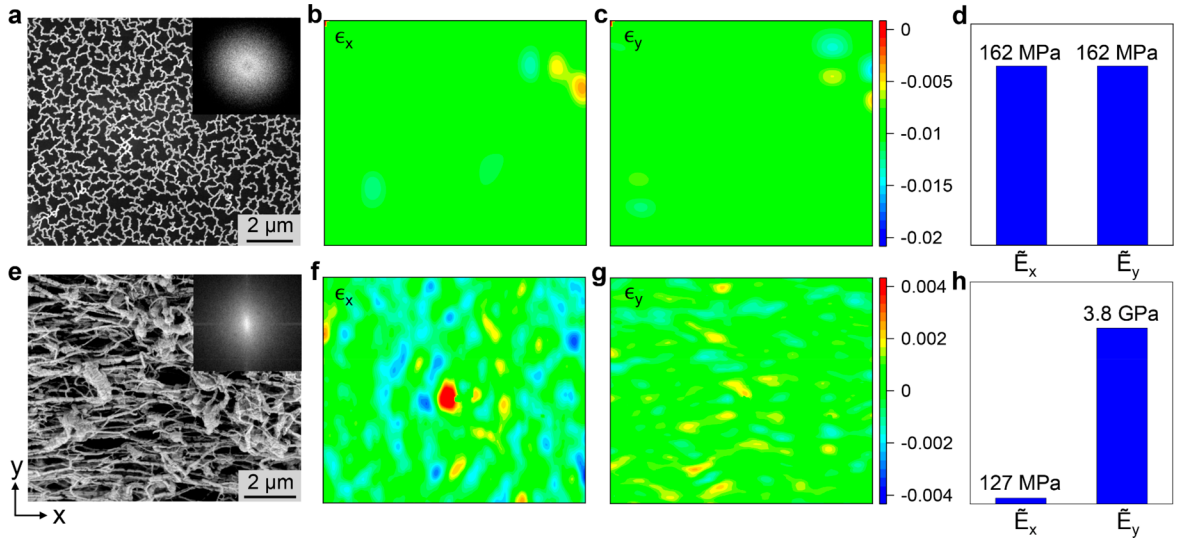

Figure 4. Measurement of biaxial stiffnesses of disordered nanomeshes. (a) SEM image and corresponding Fourier-transform image (inset) of an isotropic Au nanomesh. (b, c) Compressive strain distribution of the Au nanomesh along the *x*- and *y*-directions, analyzed by a DIC device. (d) The effective biaxial stiffnesses along the *x*- and *y*-directions of the Au nanomesh. (e) SEM image and corresponding fast Fourier transform image (inset) of an anisotropic mesh (ePTFE air filter). (f, g) Compressive strain distribution along the *x*- and *y*-directions of the ePTFE air filter, analyzed using a DIC device. (h) Effective biaxial stiffnesses along the *x*- and *y*-directions of the ePTFE air filter.

preferred when testing hydrated materials, including hydrogels and biotissues.

MODULUS MEASUREMENT OF ORDERED 2D NANOMESHES

Intrinsically soft materials aside, the Marangoni-effect-based measurement can also be applied to other materials with structure-induced stretchability such as nanomeshes. Nanomeshes with different topographies differ greatly in their mechanical properties. Here, a series of Au nanomeshes with ordered structures were prepared by electron beam lithography with a ligament width of 170 nm and a thickness of 20 nm. These ordered Au nanomeshes in Figure 3a−c(i) are staggered rectangular meshes of aspect ratios m/n = 2, 4, and 6, with m and n being the length and width of a unit cell, respectively. The ordered Au nanomesh (m/n = 4) in Figure 3d(i) is an ordinary rectangular mesh without a stagger. In contrast, the nanomeshes shown in Figure 3a−c(i) are prone to deform in the staggered direction (x-direction) and more rigid in the perpendicular direction (y-direction), exhibiting significant anisotropy with drastically different Young's moduli along the two directions, $E_x \ll E_y$. Subject to equibiaxial stress σ, the strain in the more stretchable direction

$$\epsilon_x = \frac{\sigma}{E_x} - \nu_{xy}\frac{\sigma}{E_y} \approx \frac{\sigma}{E_x} \tag{5}$$

The Poisson effect can be safely ignored as E_y is orders of magnitude larger than E_x, and the Poisson ratio is finite $\nu_{xy} \sim 1$. At small deformations, the stress−strain relation is close to linear.

The loading was applied by adding a surfactant to water to decrease surface tension. The addition of an excessive amount of surfactant leads to a dramatic decrease in surface tension, down to 33 mN·m^{-1} at saturation, resulting in a tunable range of 38 mN·m^{-1} from the initial state in pure water. The decreased surface tension shrinks the nanomesh. The mean in-plane strains are calculated from the displacements of markers on the mesh (Figure 3a−d(ii) and Figure S6). Both experimental and finite element (Figure S7) results show a close-to-uniform distribution of the mean strains calculated from the mesh grid. For the staggered rectangular meshes, the larger the aspect ratio, the larger the strain ϵ_x (ϵ_x corresponding to m/n of 6, 4, and 2 are 2.8%, 2.4%, and 0.4%, respectively). Nevertheless, the strains in nonstaggered rectangular meshes are relatively small, ~5.1×10^{-4}. According to eq 5, the Young's moduli in the x-direction of the four nanomeshes are obtained as 473.8 MPa, 78.6 MPa, 68.6 MPa, and 3.72 GPa (Figure 3a−d(iii)).

STIFFNESS MEASUREMENT OF DISORDERED 2D NANOMESHES

Disordered nanomeshes generally exhibit isotropic in-plane mechanical properties. The scanning electron microscopy image and its Fourier transform image of the Au nanomesh show a random structure (Figure 4a). The Au nanomesh shrinks biaxially when an excessive amount of surfactant solution is added to reach saturation (γ_s = 33 mN·m^{-1}). Digital image correlation (DIC) analysis shows that the Au nanomesh has uniform and isotropic shrinkage with $\epsilon_x = \epsilon_y$ = 0.9% (Figure 4b,c).

In general, the effective biaxial stiffnesses can be calculated from the differential surface tension and measured strains as

$$\begin{cases} \tilde{E}_x \equiv \dfrac{1}{\frac{1}{E_x} - \frac{\nu_{xy}}{E_y}} = \dfrac{\gamma_w - \gamma_s}{t\epsilon_x} \\ \tilde{E}_y \equiv \dfrac{1}{\frac{1}{E_y} - \frac{\nu_{xy}}{E_x}} = \dfrac{\gamma_w - \gamma_s}{t\epsilon_y} \end{cases} \tag{6}$$

Especially, in the case of an isotropic Au nanomesh,

$$\tilde{E}_x = \tilde{E}_y = \frac{E}{1-\nu} = \frac{\gamma_w - \gamma_s}{t\epsilon} \tag{7}$$

Here, the effective biaxial stiffness of the isotropic Au nanomesh is determined to be 162 MPa (Figure 4d).

https://doi.org/10.1021/acs.nanolett.4c00702
Nano Lett. 2024, 24, 4012−4019

Some special disordered materials are anisotropic, and their stiffness can also be assessed by using the same method. For example, a piece of expanded polytetrafluoroethylene (ePTFE) air filter (thickness: 500 nm) exhibits obvious anisotropy (Figure 4e). The DIC-based measurements determine the axial strains of the air filter, $\epsilon_x = 6 \times 10^{-4}$ and $\epsilon_y = 2 \times 10^{-5}$ (Figure 4f,g). According to eq 6, the effective biaxial stiffnesses along the two directions are 127 MPa and 3.8 GPa (Figure 4h). In brief, our method can characterize the mechanical properties of both continuous soft materials (e.g., elastomers) and non-continuous materials (e.g., meshes), while the latter can hardly be measured otherwise.

MEASUREMENT OF MECHANICAL PROPERTIES THROUGH DEFLECTION

We further propose a deflection-mode measurement over a long strip afloat for the characterization of its mechanical properties (Figure 5a). Fixed at both ends, the strip sample

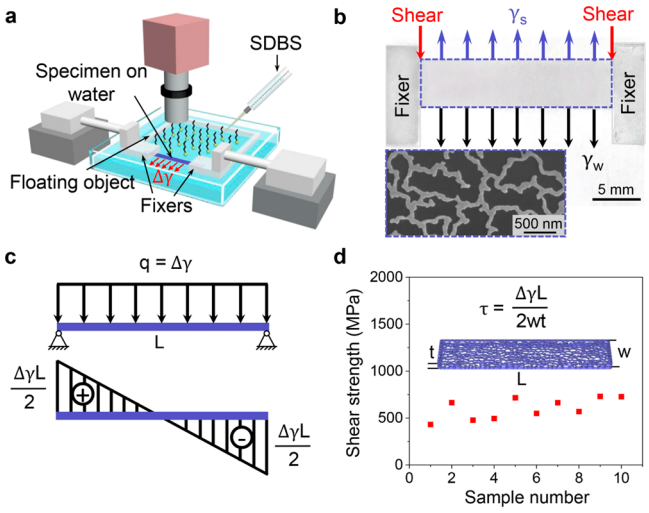

Figure 5. Measurement of the shear strength of a floating mesh using a deflection model. (a) Schematic diagram of the measurement based on a deflection model. (b) Optical image of the setup and SEM image of a fixed Au nanomesh floating on water. The Au nanomesh can be sheared under a sufficiently large surface tension difference. (c) A simplified beam model for the measurement. (d) Measured shear strength values from ten samples.

divided the water surface into two disconnected regions. Similar to the annulus sample, the strip sample is also loaded by $\Delta\gamma$ between the two regions. Consisting of a resin layer and a PDMS layer, each fixing point provides a van der Waals force to constrain the specimen, preventing slippage or delamination throughout the loading process up to fracture.[30] During the test, the surfactant was added dropwise to one side to deflect and ultimately break the specimen. Because of the in-plane and uniform load on the gas−liquid−solid interface, our method is independent of the structural continuity of the beam.

This method can also be used to measure other mechanical properties, such as the shear strength. Here, a piece of Au nanomesh made by grain boundary lithography[40] (length L, width w, and thickness t = 26 nm) was used for the measurement (Figure 5b). After the SDBS solution was added to one pool, its surface tension decreased from γ_w to γ_s, while the other side remains γ_w. Therefore, the in-plane and uniform load (q) applied to the mesh is equal to $\Delta\gamma$. With a relatively short span, a beam deflects insignificantly and is more susceptible to shear (Figure 5c), with average shear stress over the cross section

$$\tau = \frac{\Delta\gamma L}{2wt} \tag{8}$$

During the experiment, the SDBS solution was added gradually dropwise. At a sufficiently large $\Delta\gamma$, the mesh breaks by shearing at both ends (Movie S2), and the shear strength can thus be obtained from the value of the shear stress at rupture. Using this method, the shear strength of the Au nanomesh tested was determined to be 603 MPa (Figure 5d and Table S3).

The Marangoni-effect-based measurement presents certain advantages over other methods but also has its limitations. The widely used conventional mechanical tests have a limitation on specimen size. The wrinkle-based method works for ultrathin films of a wide range of materials by picking a substrate of appropriate stiffness but is only applicable to modulus measurement and on homogeneous materials. Indirect methods, such as indentation and the bulge test, are inapplicable to the average properties of heterogeneous materials, such as meshes or porous materials. Neither are they applicable to anisotropic materials.

The Marangoni-effect-based method captures the in-plane deformation of floating materials to determine their mechanical properties. This method does not require a substrate and is applicable to materials that are either homogeneous or heterogeneous, isotropic, or anisotropic. However, this method also has its limitations: it can test floating materials only and is not applicable to water-solvable or hygroscopic materials.

In summary, this work proposes a Marangoni-effect-based method to characterize the mechanical properties of soft and thin layers. The method uses the change in the surface tension of water to load the specimens. The method is first verified through the measurements of the elastic moduli of soft elastomers including PDMS and Ecoflex and then used to measure the modulus and shear strength of different types of nanomeshes, which were otherwise impossible to measure. It could potentially fill the gap in the measurement techniques, especially for measuring the mechanical properties of heterogeneous, porous, or ultrathin materials. This method is also expected to be applicable to various other materials, including biotissues, two-dimensional structures, assemblies, and 2D materials (e.g., graphene).

METHODS

Preparation of the PDMS Ring. Eight grams of PDMS (polydimethylsiloxane Sylgard 184, from Dow Corning Co., Ltd., USA) with a base to curing agent mass ratio of 20:1 was prepared and completely dissolved into 24 g of *n*-hexane (AR, 99 wt %, from Aladdin Industrial Corporation), then spin-coated (5000 rpm, 60 s) on a tattoo paper (a flat hydrosol layer adhesive on paper, 70 mm × 70 mm), and cured at 80 °C for 2 h. A PDMS ring with an inner diameter of 21 mm and an outer diameter of 25 mm was cut and transferred to a water surface with a diameter of 50 mm and a water depth of 10 mm. The thickness of the PDMS ring was 3.11 μm. The method was also applied for the preparation of Ecoflex 0010 (Smooth-On, PA, USA).

Measurement of Young's Moduli of PDMS Samples. During the experiment, the surface tension of water was controlled by changing the concentration of SDBS (sodium

https://doi.org/10.1021/acs.nanolett.4c00702
Nano Lett. 2024, 24, 4012−4019

dodecylbenzenesulfonate, AR, 95 wt %, from Aladdin Industrial Corporation). The added volume of the SDBS solution was fixed at 15 μL, and the data are shown in Table S1. Each test was repeated 10 times.

Preparation of Ordered Au Nanomeshes and Measurement of Biaxial Strains. The ordered Au nanomeshes with randomly distributed marks (Figure S7) were fabricated on a SiO_2-coated (120 nm) silicon substrate by using standard electron-beam lithography, gold film deposition (20 nm), and a lift-off process. Next, the specimens were transferred to pure water. When SDBS solution was added, the deformation of the floating Au nanomesh was captured using a microscope (Zeiss LSM-800). The coordinates of each mark in the ordered Au nanomeshes on the water surface and SDBS surface were measured, and the local strains were determined by the length change between adjacent marks.

Finite Element (FE) Simulations. Computational analyses were carried out using commercial FE software (SIMULIA Abaqus) to simulate the deformation of PDMS and Ecoflex. All of the geometric and material parameters were experimentally determined. The simulations were conducted in two steps using the procedure type Static and General to reproduce the experimental procedure. In the first step, a uniform line load, set to the surface tension of water, was applied to all of the edges of the sample. In the second step, the line load was reduced at the inner edges of the sample to mimic the effect of the surfactant.

Characterizations. The surface tension of the liquid was measured using a surface tensiometer (JYW-200B, Deka Precision Measuring Instrument Co., Ltd.). The uniaxial tension of PDMS specimens was carried out over a dynamic mechanical analysis machine (XLD-20E, Jingkong Mechanical Testing Co., Ltd.). The SEM images were taken under a scanning electron microscope (TESCAN). The optical images were taken using a Zeiss LSM-800 confocal microscope. The field strain of anisotropic nanomeshes in Figure 3 was obtained through DIC (vic-3D, Correlated Solutions, Inc.).

■ ASSOCIATED CONTENT

Supporting Information

The Supporting Information is available free of charge at https://pubs.acs.org/doi/10.1021/acs.nanolett.4c00702.

Demonstration of the friction test of a floating specimen on water or on SDBS, SDBS diffusion, the surface tension test, stress−stretch relation from simulation and material model, comparison of Marangoni-effect-based measurement and the conventional uniaxial tension test of Ecoflex, fabrication of ordered Au nanomeshes, finite element simulation of a nanomesh shrinkage by the Marangoni effect, table of detailed data for PDMS ring expansion, Ecoflex ring expansion, and shear of Au nanomeshes (PDF)

Movie of a PDMS ring expansion (Movie S1) (MP4)

Movie of shearing a disordered Au nanomesh (Movie S2) (MP4)

■ AUTHOR INFORMATION

Corresponding Authors

Yan Wang − *Department of Materials Science and Engineering, Southern University of Science and Technology, Shenzhen, Guangdong 518055, China; Department of Physics, School of Physics and Materials Science, Nanchang University, Nanchang, JiangXi 330031, China*; Email: wangyanq@ncu.edu.cn

Wei Hong − *Department of Mechanics and Aerospace Engineering, Southern University of Science and Technology, Shenzhen, Guangdong 518055, China*; orcid.org/0000-0001-6598-3456; Email: hongw@sustech.edu.cn

Chuan Fei Guo − *Department of Materials Science and Engineering, Southern University of Science and Technology, Shenzhen, Guangdong 518055, China*; orcid.org/0000-0003-4513-3117; Email: guocf@sustech.edu.cn

Authors

Biqi Shao − *Department of Materials Science and Engineering, Southern University of Science and Technology, Shenzhen, Guangdong 518055, China*

Jia Song − *Department of Materials Science and Engineering, Southern University of Science and Technology, Shenzhen, Guangdong 518055, China*

Complete contact information is available at: https://pubs.acs.org/10.1021/acs.nanolett.4c00702

Author Contributions

C.F.G. and W.H. conceived the idea, designed the research, and directed the whole study. Y.W. conducted the majority of the experiments and drafted the manuscript. C.F.G. and W.H. revised the manuscript. All authors discussed the results and have given approval to the final version of the manuscript.

Notes

The authors declare no competing financial interest.

■ ACKNOWLEDGMENTS

The work was funded by the National Natural Science Foundation of China (No. 52203297, T2225017 and 52073138), Guangdong Provincial Key Laboratory Program (2021B1212040001) from the Department of Science and Technology of Guangdong Province, and the Shenzhen Sci-Tech Fund (No. KYTDPT20181011104007). The authors thank Professor Mingchao Liu and Kexin Guo for FE simulations and Professor Huigao Duan and Qing Liu from Hunan University for the help in the fabrication of ordered nanomeshes.

■ REFERENCES

(1) Song, E.; Li, J.; Won, S. M.; Bai, W.; Rogers, J. A. Materials for Flexible Bioelectronic Systems as Chronic Neural Interfaces. *Nat. Mater.* **2020**, *19* (6), 590−603.

(2) Zhou, W.; Jiang, Y.; Xu, Q.; Chen, L.; Qiao, H.; Wang, Y.-X.; Lai, J.-C.; Zhong, D.; Zhang, Y.; Li, W. Soft and Stretchable Organic Bioelectronics for Continuous Intraoperative Neurophysiological Monitoring During Microsurgery. *Nat. Biomed. Eng.* **2023**, *7* (10), 1270−1281.

(3) Madhvapathy, S. R.; Wang, J.-J.; Wang, H.; Patel, M.; Chang, A.; Zheng, X.; Huang, Y.; Zhang, Z. J.; Gallon, L.; Rogers, J. A. Implantable Bioelectronic Systems for Early Detection of Kidney Transplant Rejection. *Science* **2023**, *381* (6662), 1105−1112.

(4) Xu, C.; Solomon, S. A.; Gao, W. Artificial Intelligence-powered Electronic Skin. *Nat. Mach. Intell.* **2023**, *5* (12), 1344−1355.

(5) Jiang, Y.; Ji, S.; Sun, J.; Huang, J.; Li, Y.; Zou, G.; Salim, T.; Wang, C.; Li, W.; Jin, H. A Universal Interface for Plug-and-play Assembly of Stretchable Devices. *Nature* **2023**, *614* (7948), 456−462.

(6) Zhang, Z.; Wang, Y.; Jia, S.; Fan, C. Body-conformable Light-emitting Materials and Devices. *Nat. Photonics* **2024**, *18*, 114−126.

(7) Tashakori, A.; Jiang, Z.; Servati, A.; Soltanian, S.; Narayana, H.; Le, K.; Nakayama, C.; Yang, C.-l.; Wang, Z. J.; Eng, J. J. Capturing

Complex Hand Movements and Object Interactions Using Machine Learning-powered Stretchable Smart Textile Gloves. *Nat. Mach. Intell.* **2024**, *6*, 106−118.
(8) Shih, B.; Shah, D.; Li, J.; Thuruthel, T. G.; Park, Y.-L.; Iida, F.; Bao, Z.; Kramer-Bottiglio, R.; Tolley, M. T. Electronic Skins and Machine Learning for Intelligent Soft Robots. *Sci. Robot.* **2020**, *5*, No. eaaz9239.
(9) Yuk, H.; Wu, J.; Zhao, X. Hydrogel Interfaces for Merging Humans and Machines. *Nat. Rev. Mater.* **2022**, *7* (12), 935−952.
(10) Yang, C.; Suo, Z. Hydrogel Ionotronics. *Nat. Rev. Mater.* **2018**, *3* (6), 125−142.
(11) Deng, J.; Yuk, H.; Wu, J.; Varela, C. E.; Chen, X.; Roche, E. T.; Guo, C. F.; Zhao, X. Electrical Bioadhesive Interface for Bioelectronics. *Nat. Mater.* **2021**, *20* (2), 229−236.
(12) Wang, S.; Nie, Y.; Zhu, H.; Xu, Y.; Cao, S.; Zhang, J.; Li, Y.; Wang, J.; Ning, X.; Kong, D. Intrinsically Stretchable Electronics with Ultrahigh Deformability to Monitor Dynamically Moving Organs. *Sci. Adv.* **2022**, *8* (13), No. eabl5511.
(13) Fallegger, F.; Schiavone, G.; Lacour, S. P. Conformable Hybrid Systems for Implantable Bioelectronic Interfaces. *Adv. Mater.* **2020**, *32* (15), 1903904.
(14) Song, H.; Luo, G.; Ji, Z.; Bo, R.; Xue, Z.; Yan, D.; Zhang, F.; Bai, K.; Liu, J.; Cheng, X. Highly-integrated, Miniaturized, Stretchable Electronic Systems Based on Stacked Multilayer Network Materials. *Sci. Adv.* **2022**, *8* (11), No. eabm3785.
(15) Jiang, Y.; Zhang, Z.; Wang, Y.-X.; Li, D.; Coen, C.-T.; Hwaun, E.; Chen, G.; Wu, H.-C.; Zhong, D.; Niu, S. Topological Supramolecular Network Enabled High-conductivity, Stretchable Organic Bioelectronics. *Science* **2022**, *375* (6587), 1411−1417.
(16) Ma, Z.; Huang, Q.; Xu, Q.; Zhuang, Q.; Zhao, X.; Yang, Y.; Qiu, H.; Yang, Z.; Wang, C.; Chai, Y. Permeable Superelastic Liquid-Metal Fibre Mat Enables Biocompatible and Monolithic Stretchable Electronics. *Nat. Mater.* **2021**, *20* (6), 859−868.
(17) Liu, J.; Yan, D.; Pang, W.; Zhang, Y. Design, Fabrication and Applications of Soft Network Materials. *Mater. Today* **2021**, *49*, 324−350.
(18) Chung, J. Y.; Nolte, A. J.; Stafford, C. M. Surface Wrinkling: A Versatile Platform for Measuring Thin-film Properties. *Adv. Mater.* **2011**, *23* (3), 349−368.
(19) Huang, J.; Juszkiewicz, M.; De Jeu, W. H.; Cerda, E.; Emrick, T.; Menon, N.; Russell, T. P. Capillary Wrinkling of Floating Thin Polymer Films. *Science* **2007**, *317* (5838), 650−653.
(20) Song, J.; Feng, X.; Huang, Y. Mechanics and Thermal Management of Stretchable Inorganic Electronics. *Natl. Sci. Rev.* **2016**, *3* (1), 128−143.
(21) Guo, C. F.; Liu, Q.; Wang, G.; Wang, Y.; Shi, Z.; Suo, Z.; Chu, C.-W.; Ren, Z. Fatigue-free, Superstretchable, Transparent, and Biocompatible Metal Electrodes. *Proc. Natl. Acad. Sci.* **2015**, *112* (40), 12332−12337.
(22) Liu, Z.; Wang, H.; Huang, P.; Huang, J.; Zhang, Y.; Wang, Y.; Yu, M.; Chen, S.; Qi, D.; Wang, T. Highly Stable and Stretchable Conductive Films through Thermal-radiation-assisted Metal Encapsulation. *Adv. Mater.* **2019**, *31* (35), 1901360.
(23) Lloyd, D.; Liu, X.; Christopher, J. W.; Cantley, L.; Wadehra, A.; Kim, B. L.; Goldberg, B. B.; Swan, A. K.; Bunch, J. S. Band Gap Engineering with Ultralarge Biaxial Strains in Suspended Monolayer MoS_2. *Nano Lett.* **2016**, *16* (9), 5836−5841.
(24) Nicholl, R. J.; Conley, H. J.; Lavrik, N. V.; Vlassiouk, I.; Puzyrev, Y. S.; Sreenivas, V. P.; Pantelides, S. T.; Bolotin, K. I. The Effect of Intrinsic Crumpling on the Mechanics of Free-standing Graphene. *Nat. Commun.* **2015**, *6* (1), 1−7.
(25) Koenig, S. P.; Boddeti, N. G.; Dunn, M. L.; Bunch, J. S. Ultrastrong Adhesion of Graphene Membranes. *Nat. Nanotechnol.* **2011**, *6* (9), 543−546.
(26) Cui, T.; Mukherjee, S.; Sudeep, P. M.; Colas, G.; Najafi, F.; Tam, J.; Ajayan, P. M.; Singh, C. V.; Sun, Y.; Filleter, T. Fatigue of Graphene. *Nat. Mater.* **2020**, *19* (4), 405−411.
(27) Lipatov, A.; Lu, H.; Alhabeb, M.; Anasori, B.; Gruverman, A.; Gogotsi, Y.; Sinitskii, A. Elastic Properties of 2D $Ti_3C_2T_x$ Mxene Monolayers and Bilayers. *Sci. Adv.* **2018**, *4* (6), No. eaat0491.
(28) Yang, Y.; Li, X.; Wen, M.; Hacopian, E.; Chen, W.; Gong, Y.; Zhang, J.; Li, B.; Zhou, W.; Ajayan, P. M. Brittle Fracture of 2D $MoSe_2$. *Adv. Mater.* **2017**, *29* (2), 1604201.
(29) Cao, K.; Feng, S.; Han, Y.; Gao, L.; Ly, T. H.; Xu, Z.; Lu, Y. Elastic Straining of Free-Standing Monolayer Graphene. *Nat. Commun.* **2020**, *11* (1), 284.
(30) Kim, J.-H.; Nizami, A.; Hwangbo, Y.; Jang, B.; Lee, H.-J.; Woo, C.-S.; Hyun, S.; Kim, T.-S. Tensile Testing of Ultra-thin Films on Water Surface. *Nat. Commun.* **2013**, *4* (1), 2520.
(31) Iguiñiz, N.; Frisenda, R.; Bratschitsch, R.; Castellanos-Gomez, A. Revisiting the Buckling Metrology Method to Determine the Young's Modulus of 2D Materials. *Adv. Mater.* **2019**, *31* (10), 1807150.
(32) Li, T.; Suo, Z.; Lacour, S. P.; Wagner, S. Compliant Thin Film Patterns of Stiff Materials as Platforms for Stretchable Electronics. *J. Mater. Res.* **2005**, *20* (12), 3274−3277.
(33) Chen, X.; Vlassak, J. J. Numerical Study on the Measurement of Thin Film Mechanical Properties by Means of Nanoindentation. *J. Mater. Res.* **2001**, *16* (10), 2974−2982.
(34) Kim, H.; Muller, K.; Shardt, O.; Afkhami, S.; Stone, H. A. Solutal Marangoni Flows of Miscible Liquids Drive Transport without Surface Contamination. *Nat. Phys.* **2017**, *13* (11), 1105−1110.
(35) Lyu, L. X.; Li, F.; Wu, K.; Deng, P.; Jeong, S. H.; Wu, Z.; Ding, H. Bio-inspired Untethered Fully Soft Robots in Liquid Actuated by Induced Energy Gradients. *Natl. Sci. Rev.* **2019**, *6* (5), 970−981.
(36) Lee, B.-B.; Chan, E.-S.; Ravindra, P.; Khan, T. A. Surface Tension of Viscous Biopolymer Solutions Measured Using the Du Nouy Ring Method and the Drop Weight Methods. *Polym. Bull.* **2012**, *69*, 471−489.
(37) Dick, C. P.; Korkolis, Y. P. Mechanics and Full-field Deformation Study of the Ring Hoop Tension Test. *Int. J. Solids. Struct.* **2014**, *51* (18), 3042−3057.
(38) Kim, B.; Lee, S. B.; Lee, J.; Cho, S.; Park, H.; Yeom, S.; Park, S. H. A Comparison among Neo-Hookean Model, Mooney-Rivlin Model, and Ogden Model for Chloroprene Rubber. *Int. J. Pr. Eng. Man.* **2012**, *13*, 759−764.
(39) Li, L.; Alsharif, N.; Brown, K. A. Confinement Induced Stiffening of Elastomer Thin Films. *J. Phys. Chem. B* **2018**, *122* (47), 10767−10773.
(40) Guo, C. F.; Sun, T.; Liu, Q.; Suo, Z.; Ren, Z. Highly Stretchable and Transparent Nanomesh Electrodes Made by Grain Boundary Lithography. *Nat. Commun.* **2014**, *5* (1), 3141.

https://doi.org/10.1021/acs.nanolett.4c00702
Nano Lett. 2024, 24, 4012−4019